Journal of Alloys and Compounds 552 (2013) 329–335

Contents lists available at SciVerse ScienceDirect

Journal of Alloys and Compounds

journal homepage: www.elsevier.com/locate/jalcom

Structural characterizations of Cu_3Pt electrocatalyst featuring Pt-rich surface layers synthesized via mechanical alloying and selective dissolution routes

Yi-Fan Hsieh [a], Yu-Chi Hsieh [a], Yuan-Chieh Tseng [a,*], Pu-Wei Wu [a], Cheun Guang Chao [a], Pang Lin [a], Jyh-Fu Lee [b]

[a] Department of Materials Science and Engineering, National Chiao Tung University, Hsin-Chu 30010, Taiwan, ROC
[b] National Synchrotron Radiation Research Center, Hsin-Chu 30076, Taiwan, ROC

ARTICLE INFO

Article history:
Received 18 July 2012
Accepted 20 October 2012
Available online 29 October 2012

Keywords:
Electrocatalyst
Mechanical alloying
Selective dissolution
Dealloying
XAFS
XANES

ABSTRACT

We demonstrate a selective electrochemical dissolution route to prepare Cu_3Pt catalysts featuring Pt-rich surface layers (Cu_3Pt-Pt rich surface) from mechanically alloyed Cu_3Pt. These catalysts were investigated by X-ray diffraction and X-ray absorption spectroscopy, and were subjected to electrochemical analyses to evaluate their catalytic properties. With appropriate anodization, Cu_3Pt entered an oxygen-evolving regime where the corrosive dissolution of Cu dominated the reaction. Selective dissolution was carried out to prepare Pt-rich layers at the surface, while Cu_3Pt was left unreacted at the core. An increase in the anodization duration modified the sample morphology, with the redistribution of Pt atoms to thicken the surface layers. A charge transfer from Pt to Cu accompanied the structural transition from Cu_3Pt to Cu_3Pt-Pt rich surface upon selective dissolution, rendering the sample to be electronically similar to a metal Pt. However, compared to the metal Pt and conventional Pt-based catalysts, the proposed structure is a more economical catalyst for direct methanol fuel cell, with less need of Pt in raw material but increased electrochemical surface area by exposing enormous Pt at the surface with an increase in the anodization duration.

1. Introduction

Direct methanol fuel cell (DMFC) has attracted considerable attention recently as a power source for portable electronics [1–7]. Among many electrocatalysts explored for DMFC, Pt and its alloys have received the most scrutiny because they demonstrate impressive catalytic activity for methanol electro-oxidation and reasonable corrosion resistance [8–13]. It is known that Pt itself suffers from CO poisoning during successive oxidation of methanol because the $(CO)_{ad}$ bonds tightly to the Pt atoms. To circumvent this undesirable behavior, a common strategy is to alloy Pt with other hydrophilic elements. This enables the $(CO)_{ad}$ to react with $(OH)_{ad}$ forming CO_2, so the Pt surface can be recovered for repeated catalytic actions. To date, binary and ternary alloys such as PtRu, [6,7] PtRuP [10], PtRuC [11], PtNi [12] and PtAu [13] have been explored with various results. Since the alloyed electrocatalysts often involve noble metals, it becomes rather expensive to fabricate them in a homogeneous phase, with the knowledge that only the surface atoms matter. Therefore, to reduce cost and improve catalyst utilization, there is a significant drive toward developing desirable core-shell structure in which the catalytic constituent occupies the shell layer while the inert one makes up the core.

In the literature, the formation of core-shell structure can be achieved via a variety of synthetic routes including sequential chemical reduction [14,15], underpotential deposition [16–18], galvanic displacement [19–22], and selective dissolution (dealloying), etc. [23–27]. Among these formation methods, the dealloying process is considered the simplest because it starts from the preparation of homogeneous alloy followed by selective removal of corrosion-prone element, leaving the inert one intact. The mechanism behind this is that each element has distinct redox potential and when an alloy is exposed to a suitable electrolyte, only the element having a smaller redox potential (less noble) would experience corrosive dissolution, whereas the element with a larger redox potential is preserved. Previously, Sieradzki [28] proposed a percolation theory in which the selective dissolution occurs exclusively in the continuous regime of less noble element as the electrolyte is only able to penetrate via this route to the area underneath the surface. With increasing dissolution, the exposed area underneath the surface becomes larger, and the remaining corrosion resistant atoms would undergo surface diffusion rendering progressively larger internal pores. Therefore, careful implementation of dealloying process not only alters the alloy composition but also produces

* Corresponding author. Address: Department of Materials Science and Engineering, National Chiao Tung University, 1001 Ta Hsueh Road, Hsinchu, Taiwan 30010, ROC. Tel.: +886 3573 1898; fax: +886 3572 4727.
E-mail address: yctseng21@mail.nctu.edu.tw (Y.-C. Tseng).

0925-8388/$ - see front matter © 2012 Elsevier B.V. All rights reserved.
http://dx.doi.org/10.1016/j.jallcom.2012.10.098

substantially large surface area and porosity. These unique characteristics are rather appealing attributes for desirable electrocatalysts.

To prepare samples for dealloying treatments, it is necessary to select constituents with a notable difference in redox potentials and to prepare them in a homogeneous phase. Previously, we utilized a mechanical alloying approach to fabricate electrocatalysts with multiple constituents [29]. The mechanical alloying method is a simple process involving repeated ball-milling to forge individual metallic powders into alloyed grains/particulates. In this process, the alloyed phase may not represent a thermodynamic stable phase so that the mechanical alloying process indeed offers a greater freedom in composition selection. The mechanical alloying has also been employed to prepare electrocatalysts for DMFCs by other groups. For example, Denis et al. [30] synthesized 4 nm PtRu via the mechanical alloying route and confirmed its notable CO resistance. In addition, Barranco et al. [31] prepared amorphous $Ni_{59}Nb_{40}Pt_{0.6}Ru_{0.4}$ and $Ni_{59}Nb_{40}Pt_{0.6}Sn_{0.4}$ electrocatalyts and explored their CO resistances. Dievaraj et al. [32] carried out ball milling to produce PtNi and found a better catalytic activity than commercially available Pt.

Motivated by these pioneering works, here we prepared a core-shell Cu_3Pt-$CuPt_3$ (Cu_3Pt@$CuPt_3$) structure via mechanical alloying followed by selective dissolution. Micrometer-sized stoichiometric Cu_3Pt particles were prepared by ball milling of Cu and Pt powders for an extended period to form a single FCC solid solution. Subsequently, the Cu_3Pt was subjected to anodic polarization at 1.6 V for different durations to selectively dissolve Cu from Cu_3Pt; this treatment resulted in the formation of Pt-rich layers at the surface, forming a structure of Cu_3Pt-Pt rich surface. The structure was subjected to X-ray diffraction (XRD) analysis for phase confirmation. Afterwards, X-ray absorption fine structure (XAFS) analysis was carried out to probe the electronic states and coordination environment surrounding the Pt and Cu atoms, so the interplays between Cu and Pt that evolved with the formation of Cu_3Pt-Pt rich surface were elucidated. Combining XAFS with scanning electron microscopy (SEM) and XRD, we found that the proposed structure exhibited largely Pt characteristics at surface that was likely to promote the catalytic reactions. This result ought to inspire further researches concerning the potential applications for DMFC from the viewpoint of structural engineering on nano scale.

2. Experimental

The Cu_3Pt particles were obtained using a mechanical alloying process in which powders of Cu (99.9 wt.%; 45 μm) and Pt (99.9 wt.%; 15 μm) were mixed at a molar ratio of 3:1 in a nitrogen-filled glove box followed by intense milling in a planetary high-energy ball mill in a 10 min milling and 10 min resting sequence. In the ball-milling process, the weight ratio for the ball/powder was 20. The milling ball was made of agate and its diameter was 3 mm. A planetary high-energy ball mill was used with a rotation speed at 250 rpm. Subsequently, the as-synthesized powders were deposited onto a carbon support for selective dissolution. First, 7.91 mg of Cu_3Pt, 6.33 mg of carbon black (Vulcan XC72R), and 31.64 mg of Nafion ionomer (5 wt.%) were mixed in 5 mL ethanol and the mixture underwent ultrasonication for 60 min to render a uniform dispersion. Afterward, the dispersion was deposited onto a carbon cloth (2×2 cm^2) atop a hotplate to allow slow evaporation of ethanol. Upon drying, the effective loading for the Cu_3Pt on the carbon cloth was 2 mg/cm^2. Prior to the dealloying treatment, the Cu_3Pt-decorated electrode was subjected to an anodic polarization between 0.5 and 1.8 V at 1 mV/s in a 0.5 M H_2SO_4 aqueous solution in order to determine active and passive voltage regimes. During the dealloying treatment, the sample was subjected to 1.6 V anodization for various durations where the total coulomb charge was kept at 3, 6, and 12 C, respectively.

To evaluate the electrochemical surface area (ESA) for the dealloyed Cu_3Pt, we conducted cyclic voltammetric scans (CV) [33,34] for potential between −0.2 and 0.9 V in 0.5 M H_2SO_4 at 20 mV/s. The ESA was calculated from the integrated charge in the hydrogen desorption region in the second cycle. Selective dissolution and ESA measurements were carried out at 25 °C using a Solartron SI 1287 potentiostat. The electrolyte was purged with nitrogen for 15 min to remove any dissolved oxygen before meaningful data were recorded. The Ag/AgCl and Pt foil (8 cm^2) were adopted as the reference and counter electrodes, respectively. The area for the working electrode was 1 cm^2.

X-ray diffraction (XRD) was performed with CuKα radiation (λ = 1.5418 Å) (Siemens D5000) to monitor the alloying progress during the milling of Cu and Pt powders. Morphologies of the Cu_3Pt before and after dealloying treatment were observed by SEM (JSM-6500F). An energy dispersive X-ray spectrometer (EDX) was used to analyze the composition of Cu_3Pt after dealloying for 3, 6, and 12 C. We also employed inductively coupled plasma mass spectrometry (ICP-MS) to determine the exact composition of Cu_3Pt after dealloying treatments by dissolving the samples in a solution containing HCl, HNO_3, and HF of 2:2:1 volume ratio at 180 °C.

Cu *K*-edge and Pt L_{III}-edge XAFS spectra were recorded with a transmission mode at BL17C, National Synchrotron Radiation Research Center, Taiwan. XAFS data were analyzed using ATHENA and ARTEMIS interfaces of the IFEFFIT package [35]. Each raw XAFS spectrum was pre-edge subtracted to remove the background and then was normalized with respect to the edge jump step. The normalized spectrum was converted into k-space and was k-weighted properly, and finally was Fourier transformed (FT) into r-space, all using the ATHENA interface. The coordination number and bond distance were fitted via the ARTEMIS interface, where the assigned FEFF paths were related to the photoelectron backscattering contributions from the neighboring atoms. In detail, a FEFF path was characterized with the related inter-atomic distance (bond length) for single scattering path, and the amplitude and phase-shift functions of a specific atomic pair. The path parameters included degeneracy of path, passive electron reduction factor, energy shift, bond length change, and mean squared displacement. In general, the *R*-factor of the ARTEMIS is expected to be no more than 5% for a good fitting, and the *R*-factors of our fitting results were all in a close proximity to this value.

3. Results and discussion

Fig. 1 displays the XRD patterns for as-received Pt and Cu powders, as well as mixtures of Pt and Cu after ball milling for 8 and 72 h, respectively. As shown, both Pt and Cu revealed an FCC lattice with characteristic peaks clearly identified. For example, the diffraction peaks of (111), (200), and (220) for Pt were recorded at 39.76, 46.24, and 81.29°, respectively. Since the atomic radius and hence the lattice of Cu are smaller than those of Pt, the corresponding peaks of (111), (200), and (220) were shifted to higher angles at 43.3, 50.43, and 74.13°, respectively. Their positions and relative intensities were consistent with those for standard JCPDS samples (Pt: 88–2343; Cu: 85–1326). After 8 h of ball milling, there appeared a notable shift for both samples in which the diffraction peaks of Pt were moved to higher angles while the Cu counterparts were relocated to lower ones. This evidence along with slight broadening of the diffraction peaks suggests that moderate alloying between Pt and Cu has occurred, leading to individual Cu-rich and Pt-rich grains. After 72 h, a single set of FCC diffraction pattern was observed and the corresponding (111), (200), and (220) planes were recorded at 42.24, 49.19, and 72.12°, respectively. Accordingly, the lattice parameter for the resultant Cu_3Pt alloy became 3.72 Å which was properly located between the values for Pt (3.97 Å) and Cu (3.615 Å) as expected from Vegard's law [36]. This confirms the formation of a homogeneous solid solution. It is noted that in the Cu–Pt equilibrium phase diagram [37], Cu_3Pt might be present in a superlattice structure. However, in our case the mechanical alloying process is expected to introduce numerous defects in the Cu_3Pt lattice so that a random solid solution is more likely to form.

Fig. 2 demonstrates the polarization curve for the Cu_3Pt with applied potential between 0.5 and 1.8 V. Since the open circuit voltage for the Cu_3Pt was approximately 0.5 V, the potential range for this measurement was deliberately selected to identify active, passive, and oxygen-evolving regimes so a proper anodic polarization can be determined for dealloying treatments. As shown in Fig. 2, there appeared three distinct potential regimes with different current responses. In regime I with the potential of 0.5–0.68 V, the Cu_3Pt existed in an active state in which the current was linearly proportional to the anodic polarization [38]. Because Pt was still stable in this voltage range, corrosive dissolution of Cu was believed to be responsible for the recorded current. In regime II with potential between 0.68 and 1.28 V, the Cu_3Pt was in a passive state in which the current became inversely proportional to the anodic polarization. As a result, the corrosion of Cu was largely inhibited,

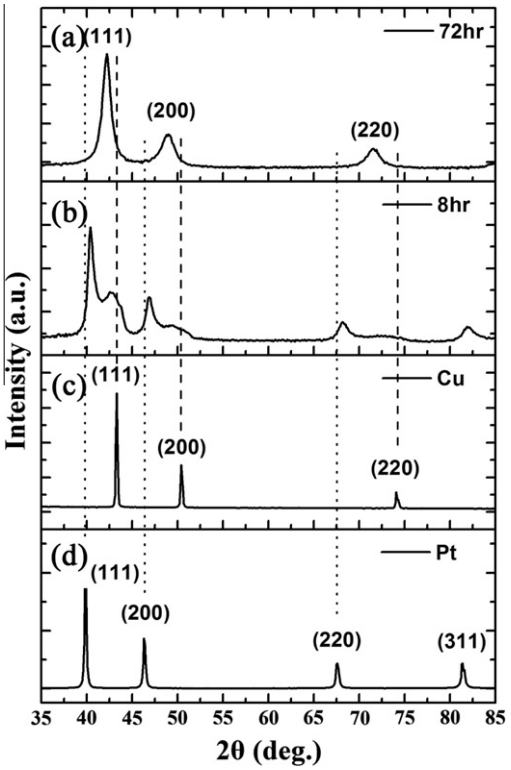

Fig. 1. XRD patterns for as-received (d) Pt and (c) Cu powders, as well as mixtures of Pt and Cu after ball milling for (b) 8 and (a) 72 h, respectively.

a fact that was attributed to excessive dissolution of Cu from the Cu_3Pt that rendered a Pt-rich surface protecting Cu underneath. According to Pugh et al. [39], in regimes I and II, moderate oxidation of Pt was still possible but its current was below 2 μA/cm^2. Therefore, the recorded current in our case was primarily due to the oxidative dissolution of Cu. For potential above 1.28 V, the sample entered an oxygen-evolving regime III in which faradaic reactions including oxygen evolution, oxidation of Pt, and corrosive dissolution of Cu were taking place simultaneously. At such severe anodic polarization, considerable oxidation loss of Pt and pitting were likely to occur which yield a rapidly increasing current. In earlier study, the oxidation of Pt and oxygen evolution reaction produced currents in the magnitude of 10 μA/cm^2. However, in Fig. 2, the current we measured was above 10 mA/cm^2. Hence, it

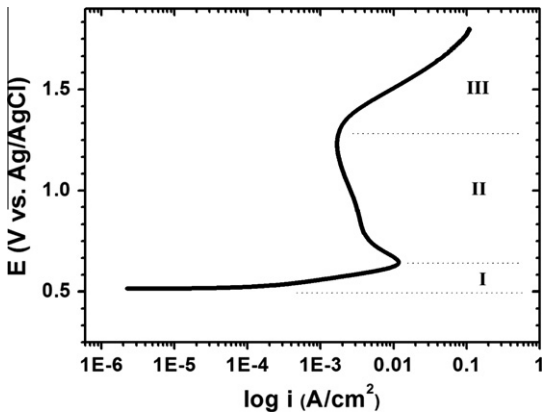

Fig. 2. The polarization curve for Cu_3Pt operated at a potential range from 0.5 to 1.8 V.

was concluded that the predominant reaction was the corrosive dissolution of Cu in the Cu_3Pt. Consequently, we selected 1.6 V as the anodizing potential for the dealloying treatment because it led to a faster Cu dissolution. Because the Cu loading on the electrode was 0.978 mg/cm^2, the complete removal of Cu required a theoretical coulomb charge of 3 C. However, since parts of the current were associated with Pt oxidation and oxygen evolution, the dealloying treatments were explored for 3, 6, and 12 C, so the degree of dealloying on the Cu_3Pt can be studied.

Fig. 3 provides the SEM images for the Cu_3Pt before and after dealloying treatments. As shown in Fig. 3(a), the as-prepared Cu_3Pt exhibited an irregular shape which was characteristic of particles derived from the mechanical alloying route. In addition, the Cu_3Pt revealed a considerable size distribution with an average value of 2.26 μm. Fig. 3(b) presents the SEM image of as-prepared Cu_3Pt in high resolution. Apparently, the surface of Cu_3Pt was reasonably flat and individual grains of Pt and Cu were not discernible, suggesting that the mechanical alloying was properly done. Fig. 3(c) demonstrates the high-resolution SEM image for Cu_3Pt after the dealloying treatment of 6 C. The surface morphology became notably rough with wide arrays of pores penetrating to the interior. These pores were believed to be caused by dissolution of Cu and Pt. In addition, individual grains of 100 nm were clearly visible. Because we selected 1.6 V for the dealloying treatment, this relatively large anodic polarization led to severe dissolution and redistribution of Pt that engendered pores of 100–300 nm.

Table 1 and Table 2 list the results on the composition analysis from EDX and ICP-MS, respectively. For the as-prepared, mechanically alloyed Cu_3Pt, both EDX and ICP-MS indicated that the atomic ratio of Cu to Pt was close to 3:1. Upon completion of dealloying treatment, the composition from EDX analysis suggests a larger loss of Cu with increasing coulomb charges. Interestingly, even after dealloying treatment for 12 C, there still existed appreciable amount of Cu at 32 at.%. A similar trend was observed in Table 2 from ICP-MS analysis. However, the exact loss of Cu in 3, 6, and 12 C treatments was significantly lower than the corresponding values in Table 1 from EDX analysis. This discrepancy was due to the difference in the measurement technique as the EDX acquires data that is only valid on surface layer of 1 μm thickness but the ICP-MS is effective for the entire sample. As a result, the EDX data were indicative of surface composition which suffered from more severe Cu loss while the Cu buried inside the Cu_3Pt was still isolated from the anodic dissolution. Correspondingly, the ICP-MS attained a larger Cu content because it measured the total Cu amount. In the following XAFS analysis, the composition from ICP-MS was used to extract relevant information in coordination number and bond distance, considering that the XAFS was taken by a transmission mode with an X-ray fully penetrating the entire sample volume.

Fig. 4 presents the XRD patterns for electrodes patterned with Cu_3Pt before and after dealloying treatments of 3, 6, and 12 C, respectively. As shown in Fig. 4, the sample before dealloying treatment revealed an FCC lattice with diffraction peaks of (111), (200), and (220) properly indexed. However, this diffraction pattern displayed moderate noises as compared to that of Fig. 1 and these noises were associated with the interference from carbon and Nafion ionomer. Once the dealloying treatment was performed, there appeared an extra diffraction peak around 40.5° and its intensity became higher as the dealloying treatment was prolonged. After treatment of 12 C, two distinct FCC phases were identified with slightly different lattice parameters. One of the FCC phases was the Cu_3Pt that was identical to that of the as-prepared sample. The other FCC phase showed a lattice parameter of 3.84 Å which was smaller than that of Pt but larger than those of Cu and Cu_3Pt. According to the Vegard's law, we reasonably surmised that this newly formed FCC phase was $CuPt_3$. In addition, this $CuPt_3$ phase

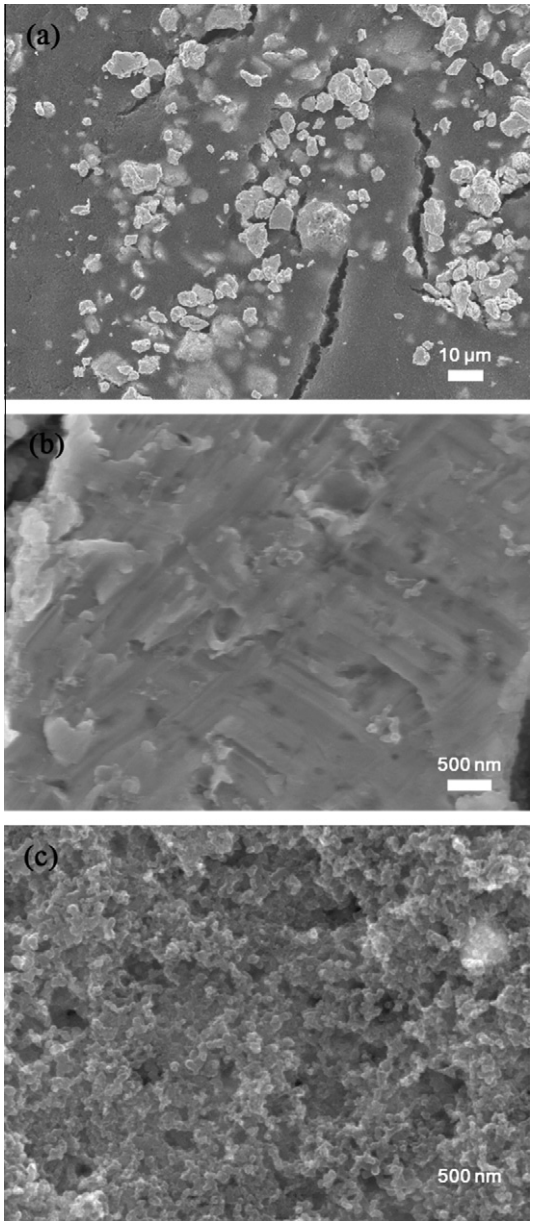

Fig. 3. The SEM images for the Cu_3Pt before dealloying treatment in (a) low magnification and (b) high magnification. (c) The high magnification SEM image of Cu_3Pt after dealloying treatment of 6 C.

Table 1
EDX results on samples before and after dealloying treatments for 3, 6, and 12 C, respectively.

	Cu (at.%)	Pt (at.%)
as-prepared	74.85	25.15
3 C	46.24	53.76
6 C	41.29	58.71
12 C	32.05	67.95

was predominantly present in the exterior surface while the Cu_3Pt phase was relatively intact at the core. In came to our attention that the XRD of the $CuPt_3$ seems to be different than that reported by E. Ahmed et al. [40] However, in the experiments of Ahmed et al., Cu and Pt were formed a continuous solid solution in all proportions. In particular, the $CuPt_3$ adopted a cubic ordered superlattice which is closely related to the structure of Cu_3Au. In their

Table 2
ICP-MS results on samples before and after dealloying treatments for 3, 6, and 12 C, respectively.

	Loading		Atomic Ratio	
	Cu (mg/cm^2)	Pt (mg/cm^2)	Cu (at.%)	Pt (at.%)
as-prepared	1.06	1.03	75.90	24.10
3 C	0.48	0.98	60.18	39.82
6 C	0.45	0.95	59.20	40.80
12 C	0.34	0.88	54.01	45.99

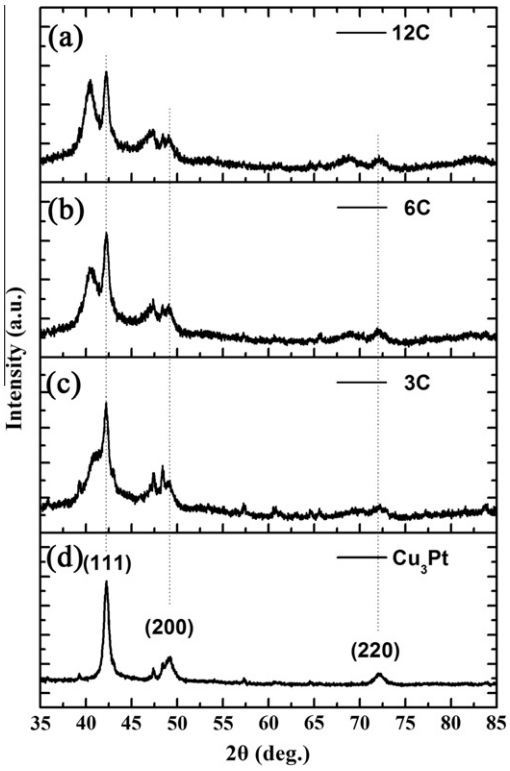

Fig. 4. The XRD patterns for electrodes patterned with (d) Cu_3Pt before and after dealloying treatments of (c) 3, (b) 6, and (a) 12 C, respectively.

experiments, they formed the $CuPt_3$ in conventional arc melting of Cu and Pt, and after solidification, an annealing step was carried out to ensure homogeneity and the presence of thermodynamic stable phase. Consequently, in their study, the (200) peak revealed the strongest diffraction signal. In contrast, in an ideal FCC structure like Pt and Cu, the strongest peak should be the (111) peak instead, according to Ref. [41,42]. In our case, we formed the $CuPt_3$ phase via electrochemical dealloying in electrolyte and no additional heat treatment was performed. As a result, we observed a random solid solution of $CuPt_3$ and relative intensity of the diffraction peaks followed those of a typical FCC phase. In addition, respective peak positions for the $CuPt_3$ were consistent with what were expected from Vegard's law.

However, we noticed the XRD peaks of $CuPt_3$ are broader compared to those of Cu_3Pt underneath. This suggests that $CuPt_3$ may not be a single phase at the surface, and a range of composition could be possible. Therefore, a Pt-rich phase is a more rigorous terminology, than $CuPt_3$, to describe the structural characteristics of the surface.

By summarizing the results from XRD, ICP-MS, EDX, and SEM, a mechanism for the structural transition from Cu_3Pt to Cu_3Pt-Pt rich surface is depicted in the schematic illustration of Fig. 5. Fig. 5(a)

describes the Cu removal on the Cu_3Pt surface resulting from dealloying, which gradually gives rise to the formation of large Pt-terminations at the surface, as illustrated in Fig. 5(b). Such mechanism is also supported by the XAFS and ESA results described below.

The Pt L_{III}-edge XAFS spectra for Pt foil, Cu_3Pt, and Cu_3Pt-Pt rich surface (3 C, 6 C, 12 C) are presented in Fig. 6(a). Fig. 6(c) highlights the X-ray absorption near edge structure (XANES) corresponding to those shown in Fig. 6(a). The XANES corresponded to the Pt $2p \rightarrow 5d$ photo-excitation process with the white-line intensity (at 11,567 eV) reflecting the available vacancy in the 5d orbital. Clearly, the Cu_3Pt exhibited suppressed white-line intensity than that of the Pt foil. This evidence indicates a charge transfer from Cu to Pt via orbital hybridization that resulted in higher d-band occupancy of Pt featuring suppressed intensity, from a metal Pt to Cu_3Pt. It is noteworthy that the Pt XANES feature was heavily suppressed for the Cu_3Pt, but turned out to be similar to the Pt foil for the Cu_3Pt-Pt rich surface, especially on the white line (at 11567 eV), because the formation of the $CuPt_3$ provided abundant Pt resource rendering the entire sample to exhibit pronounced Pt characteristics. Apparently, the dealloying treatment restored the Pt characteristics by electronically modifying the sample, making the Cu_3Pt-Pt rich surface electronically similar to a metal Pt. This signals that the formed core-shell structure could be comparable to a metal Pt in terms of the catalytic capability for DMFC, while the former is more economical than the latter by largely reducing Pt in raw material. Furthermore, compared to conventional Pt-based catalysts [6–13], our method does not require Pt to be the majority.

The FT-EXAFS spectra corresponding to Fig. 6(a) are given in Fig. 6(b), with the largest Pt FT-EXAFS magnitude obtained in the Pt foil due to high structural ordering of the metal state. Conversely, a lower FT-EXAFS magnitude typically implies a disordered local structure around the selected atomic species. In Fig. 6(b), the Pt FT-EXAFS magnitude appeared to first decrease from the Pt foil to the Cu_3Pt and further decreased with treatment by increasing coulomb charge of the Cu_3Pt. The first decrease of the Pt FT-EXAFS magnitude was arising from the structural imperfections introduced by the mechanical alloying, and the further decrease was related to the formation of Pt rich surface. In fact, the probed Pt EXAFS for Cu_3Pt-Pt rich surface was contributed by both core (Cu_3Pt; Pt poor) and surface (Pt rich) with dissimilar local structures, so the mixed ordering is expected to be poorer than the single phase Cu_3Pt. Besides, upon the formation of Pt rich surface the bond length of Pt slightly increased with FT-EXAFS peak position moving towards a larger value. Such findings are consistent with the XRD result (Fig. 4) with diffraction peaks shifting to lower angles. The long-range ordering revealed by XRD points to the increase of average d-spacing in the presence of Pt rich surface.

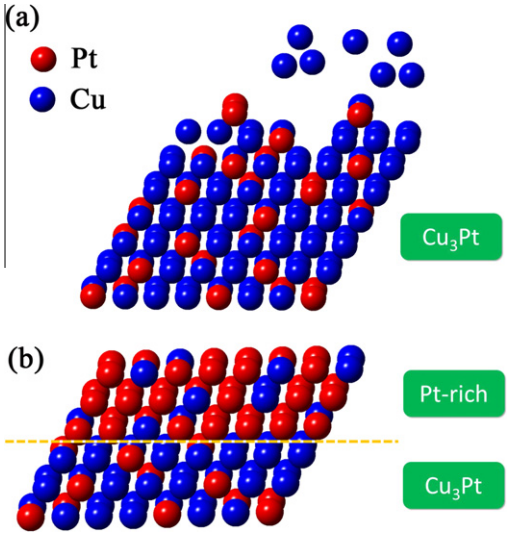

Fig. 5. Schematic illustration for (a) Cu_3Pt undergoing a dealloying process; (b) the formation of Pt rich surface after dealloying treatment.

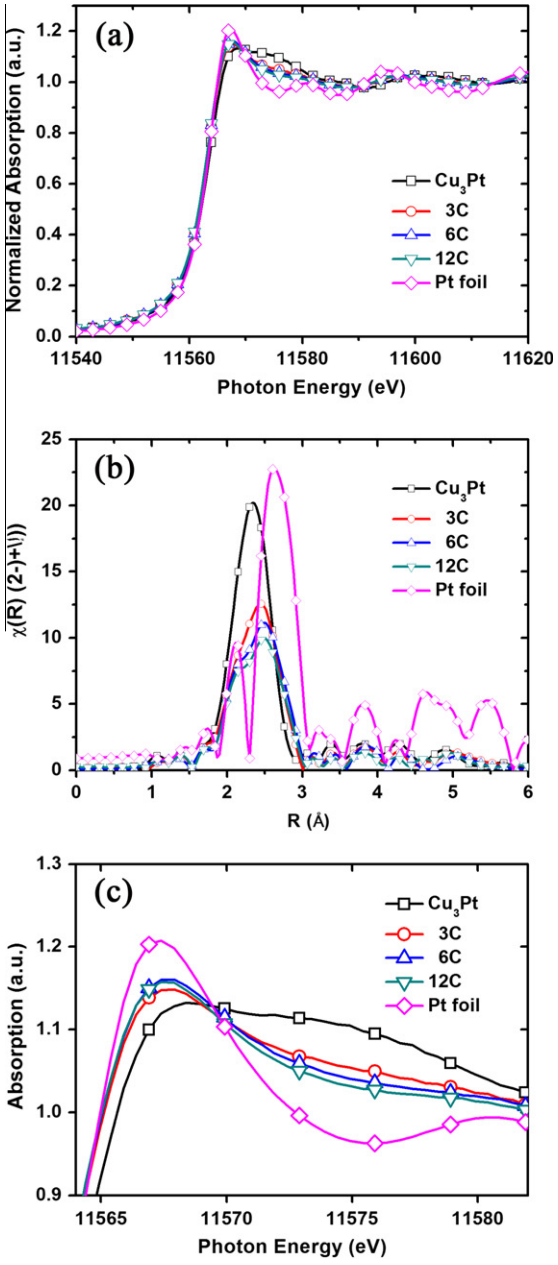

Fig. 6. (a) Normalized XAFS, (b) FT-EXAFS, and (c) XANES spectra at Pt L_{III}-edge for Cu_3Pt before and after dealloying treatments of 3, 6, and 12 C, respectively, together with the same information of a reference Pt foil.

Figs. 7(a) and (b) show the Cu K-edge XAFS and FT-EXAFS spectra, respectively, with the same sample sequence as in Fig. 6; however, a Cu foil is set as the reference. The XAFS oscillation appeared to be less altered among all samples. This suggests that the atomic environment around Cu was almost independent of various treatments, as validated by similar line-shapes of all FT-EXAFS spectra. Apparently, the local structure around Pt was more sensitive than that of Cu to the dealloying treatment, due to the fact that the deal-

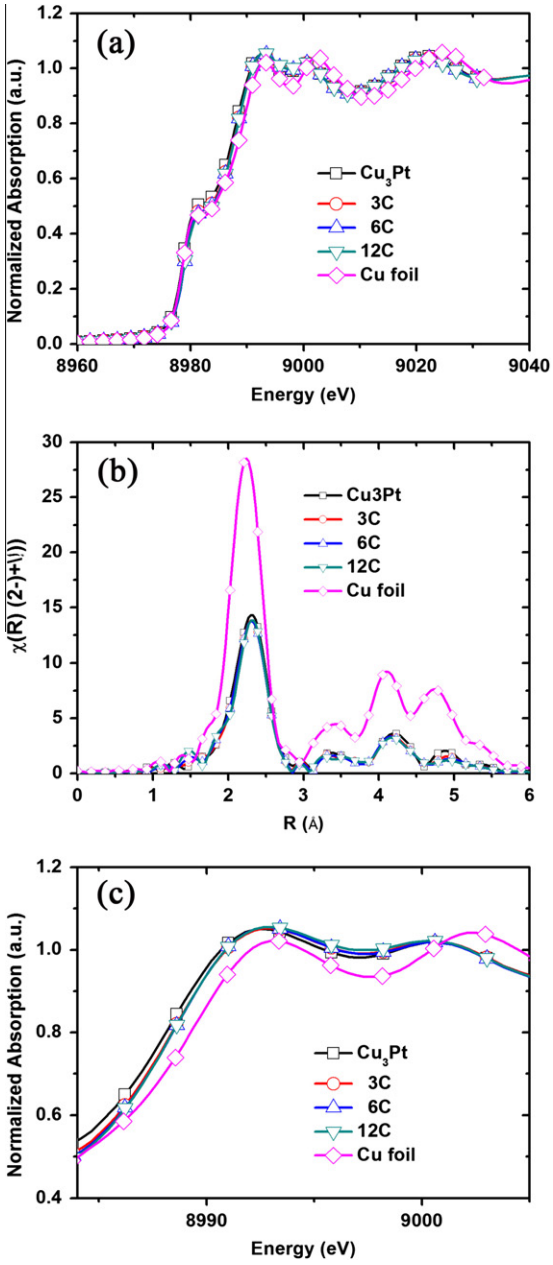

Fig. 7. (a) Normalized XAFS, (b) FT-EXAFS, and (c) XANES spectra at Cu *K*-edge for Cu_3Pt before and after dealloying treatments of 3, 6, and 12 C, respectively, together with the same information of a reference Cu foil.

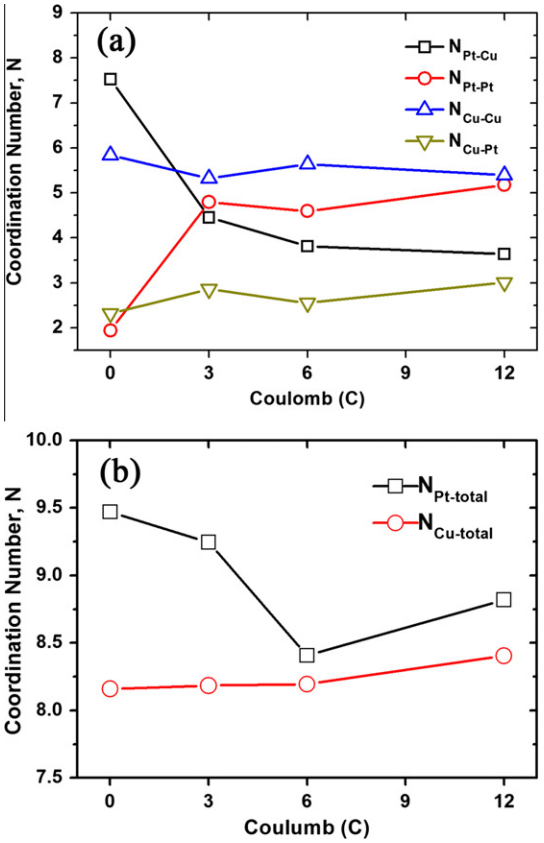

Fig. 8. (a) Coulomb charge dependencies for the coordination numbers of Pt and Cu with different surrounding atoms. Here, N_{Pt-Cu} refers to the coordination number of Pt absorbing atom surrounded by Cu, and all other notations follow the same principle. (b) Coulomb charge dependencies for the total coordination numbers of Pt and Cu.

loying treatment selectively removed Cu, substantially modifying the local environment of the adjacent Pt atom. Fig. 7(c) provides the XANES information related to the Cu 1s → 4p photo-excitation process. Regardless of a slight energy shift of the Cu foil (less than 1 eV compared to others), the XANES spectra exhibited similar line-shapes, revealing a similar electronic structure of Cu for all samples. The charge transfer was not clearly noticed at the Cu *K*-edge. Because the white-line intensity of the *K*-edge spectrum is intrinsically weak, the charge transfer effect may have been screened at the Cu *K*-edge. Since Cu is the major component in the Cu_3Pt alloy system, the charge transfer effect per Cu atom would be less pronounced than that experienced by each Pt atom. Fig. 8(a) displays the coordination number as a function of dealloying coulomb charge for Cu_3Pt, by setting Pt and Cu as the absorbing atoms. The N_{Pt-Cu} coordination decreased with the increasing coulomb charge from approximately 7.5 to 4 because of the corrosive removal of Cu. However, an opposite dependency was obtained in N_{Pt-Pt} with the coordination increasing from 2 to 5, which is attributed to the formation of Pt rich surface. Compared with Pt, Cu coordination remained almost unaltered. As the corrosion of Cu took place primarily at the sample surface, the probed Cu coordination mainly reflected the surrounding characteristics of Cu of the Cu_3Pt underneath. Fig. 8(b) summarizes the coulomb charge dependencies of the total coordination numbers of the two atomic species. A sudden decrease of Pt coordination with 6 C signals the most pronounced dealloying effect. With this charge value the $CuPt_3$ phase developed rapidly, as confirmed by the emergence of the corresponding peaks in XRD pattern (Fig. 4).

Measurements of ESA have been recognized as an effective method to determine the area of exposed Pt. Therefore, once dealloying of Cu_3Pt took place, more Pt atoms were likely to appear on the surface, resulting in a larger ESA value. Fig. 9(a) displays the CV profiles for the samples in 0.5 M H_2SO_4 aqueous solution. According to the literature, the adsorption and desorption of hydrogen occurred for potential between −0.2 and 0.1 V, and a stronger current response in this potential range suggested a larger amount of hydrogen interaction, which inferred more exposed Pt atoms on the surface. The exact ESA values were obtained by the integral area for hydrogen desorption in the anodic scan shown in Fig. 9(b). As expected, the ESA value increased with increasing dealloying coulomb charge. With 12 C in which a structure of Cu_3-Pt-Pt rich surface was formed, the ESA became significantly larger than that of Cu_3Pt before the dealloying treatment.

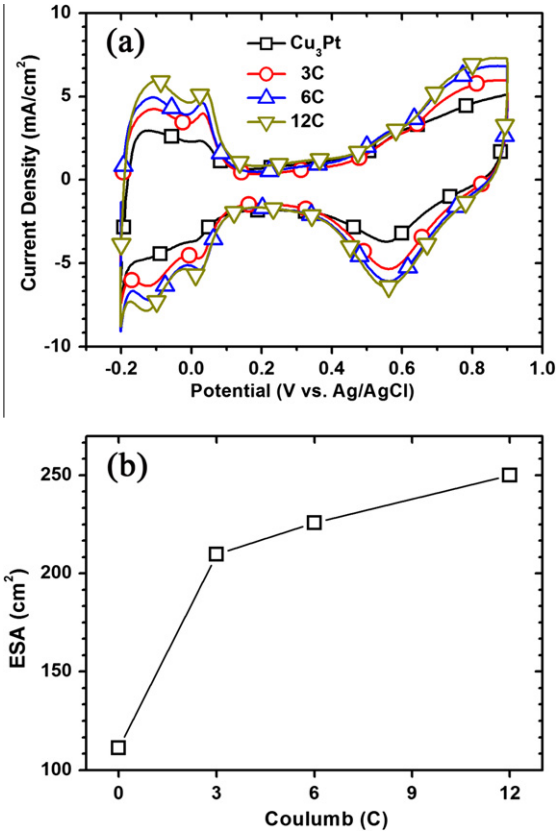

Fig. 9. (a) The CV profiles of hydrogen desorption and adsorption for the Cu_3Pt-patterned electrodes before and after dealloying treatments of 3, 6, and 12 C, respectively. (b) The corresponding ESA values obtained from the integral area of CV profiles between −0.2 and 0.1 V from (a).

4. Conclusion

We have demonstrated an electrochemical synthesis to obtain Cu_3Pt-Pt rich surface catalysts, with a Pt-rich surface developed from a Pt-poor (Cu_3Pt) one. These catalysts exhibited a tunable nature of surface, with an increase in Pt characteristics by extending the dealloying duration. X-ray absorption spectroscopy revealed that upon dealloying the catalysts were found to exhibit pronounced Pt characteristics in terms of their electronic and structural properties. Electrochemical analyses suggested that the area of the exposed Pt increased upon dealloying, which likely promoted the catalytic abilities of the sample particularly for use in direct methanol fuel cell. Systematic analyses including XRD, SEM, EDX and ICP-MS were carried out to correlate the material's properties with the varying core/shell ratio to provide nuanced understanding of the structure.

The proposed strategy in this work can be considered to be more economical than conventional methods for fabricating Pt-based catalysts, because this strategy does not lay emphasis on the use of Pt in majority. Moreover, in a broader perspective, the strategy has provided sufficient insight for the development of similar structures with other tailored properties; in other words, it has opened up opportunities for tailoring the catalytic properties of the involved constituents by manipulating the core-surface inter-dependency of the structure.

Acknowledgement

Equipment assistances from Professor George Tu and Professor Pang Lin are greatly appreciated. Financial support from the National Science Council of Taiwan (98-2221-E-009-040-MY2; 98-2112-M-009 -022 -MY3) is acknowledged.

References

[1] J. Haggin, Chem. Eng. News Archive 73 (1995) 8.
[2] A. Bo, S. Sanicharane, B. Sompalli, Q. Fan, B. Gurau, R. Liu, E.S. Smotkin, J. Phys. Chem. B 104 (2000) 7377.
[3] R.S. Jayashree, L. Gancs, E.R. Choban, A. Primak, D. Natarajan, L.J. Markoski, P.J.A. Kenis, J. Am. Chem. Soc. 127 (2005) 16758.
[4] J.L. Haan, K.M. Stafford, R.I. Masel, J. Phys. Chem. C 114 (2010) 11665.
[5] J.H. Bang, K. Han, S.E. Skrabalak, H. Kim, K.S. Suslick, J. Phys. Chem. C 111 (2007) 10959.
[6] K. Drew, G. Girishkumar, K. Vinodgopal, P.V. Kamat, J. Phys. Chem. B 109 (2005) 11851.
[7] R. Viswanathan, G.H. Liu, R.S.R. Bare, F. Modica, G. Mickelson, C.U. Segre, N. Leyarovska, E.S. Smotkin, J. Phys. Chem. B 13 (2002) 3458.
[8] K.R. Lee, M.K. Jeon, S.I. Woo, Appl. Catal. B 91 (2009) 428.
[9] Y.C. Hsieh, L.C. Chang, P.W. Wu, Y.M. Chang, J.F. Lee, Appl. Catal. B 103 (2011) 116.
[10] W.D. King, J.D. Corn, O.J. Murphy, D.L. Boxall, E.A. Kenik, K.C. Kwiatkowski, S.R. Stock, C.M. Lukehart, J. Phys. Chem. B 107 (2003) 5467.
[11] D.L. Boxall, G.A. Deluga, E.A. Kenik, W.D. King, C.M. Lukehart, Chem. Mater. 13 (2001) 891.
[12] K.W. Park, J.H. Choi, B.K. Kwon, S.A. Lee, Y.E. Sung, H.Y. Ha, S.A. Hong, H. Kim, A.J. Wieckowski, Phys. Chem. B 106 (2002) 1869.
[13] Y.Q. Wang, Z.D. Wei, L. Li, M.B. Ji, Y. Xu, P.K. Shen, J. Zhang, H.J. Zhang, Phys. Chem. C 112 (2008) 18672.
[14] G. Wang, H. Wu, D. Wexler, H. Liu, O. Savadogo, J. Alloys Comp. 503 (2010) L1.
[15] K. Vinodgopal, B. Neppolian, I.V. Lightcap, F. Grieser, M. Ashokkumar, P.V. Kamat, J. Phys. Chem. Lett. 1 (2010) 1987.
[16] D.A. Huckaby, L. Blum, Langmuir 11 (1995) 4583.
[17] J.W.F. Robertson, D.J. Tiani, J.E. Pemberton, Langmuir 23 (2007) 4651.
[18] M. Alanyalıoğlu, H. Çakal, E.A. Öztürk, Ü. Demir, J. Phys. Chem. B 105 (2001) 10588.
[19] S.Y. Sayed, F. Wang, M. Malac, A. Meldrum, R.F. Egerton, J.M. Buriak, ACS Nano 3 (2009) 2809.
[20] Y. Wang, M. Becker, L. Wang, J. Liu, R. Scholz, J. Peng, U. Gösele, S. Christiansen, D.H. Kim, M. Steinhart, Nano Lett. 9 (2009) 2384.
[21] J.H. Ai, S.P. Liu, N.A. Widharta, S. Adhikari, J.W. Anderegg, K.R. Hebert, J. Phys. Chem. C 115 (2011) 22354.
[22] P.R. Brejna, U. Sahaym, N.M. Grant, P.R. Griffiths, J. Phys. Chem. C 115 (2011) 1444.
[23] Z. Qi, C. Zhao, X. Wang, J. Lin, W. Shao, Z. Zhang, X. Bian, J. Phys. Chem. C 113 (2009) 6694.
[24] X. Wang, Z. Qi, C. Zhao, W. Wang, Z. Zhang, J. Phys. Chem. C 113 (2009) 13139.
[25] R. Morrish, A.J. Muscatm, Chem. Mater. 21 (2009) 3865.
[26] Y. Sun, Y. Xia, Nano Lett. 3 (2003) 1569.
[27] P. Strasser, S. Koh, J. Greeley, Phys. Chem. Chem. Phys. 10 (2008) 3670.
[28] K.J. Sieradzki, Electrochem. Soc. 140 (1993) 2868.
[29] Y.F. Hsieh, Y.C. Hsieh, P.W. Wu, C.H. Liao, Y.M. Chang, J. Electrochem. Soc. 157 (2010) B39.
[30] M.C. Denis, G. Lalande, D. Guay, J.P. Dodelet, R. Schulz, J. Appl. Electrochem. 29 (1999) 951.
[31] J. Barranco, P.A.R. Bifunctional, J. Power Sources 169 (2007) 71.
[32] T.C. Deivaraj, J.Y. Lee, J. Electrochem. Soc. 151 (2004) A1832.
[33] F. Jia, C. Yu, Z. Ai, L. Zhang, Chem. Mater. 19 (2007) 3648.
[34] N.S. Lawrence, L. Jiang, T.G.J. Jones, R.G. Compton, Anal. Chem. 75 (2003) 2054.
[35] http://cars9.uchicago.edu/ifeffit/.
[36] A.R. Denton, N.W. Ashcroft, Phys. Rev. A 43 (1991) 3161.
[37] K. Mitsui, M. Takahashi, T. Takezawa, Philos. Mag. Lett. 77 (1998) 49.
[38] D.V. Pugh, A. Dursun, S.G. Corcoran, J. Mater. Res. 18 (2003) 216.
[39] D.V. Pugh, A. Dursun, S.G. Corcoran, J. Electrochem. Soc. 152 (2005) B455.
[40] E. Ahmed, M. Takahashi, H. Iwasaki, K.I. Ohshima, J. Alloys Comp. 473 (2009) 1.
[41] S. Wang, S.P. Jiang, T.J. White, J. Guo, X. Wang, J. Phys. Chem. B 113 (2009) 18935.
[42] J. Ryu, H.S. Kim, H.T. Hahn, J. Electron. Mater. 40 (2011) 42.